Pergamon

Chaos, Solitons & Fractals, Vol. 10, No. 4–5, pp. 709–724, 1999

0960-0779/99/$ - see front matter

PII: S0960-0779(98)00020-4

Spatio-temporal Dynamics in Photorefractive Two-wave Mixing Configurations: the Counterpropagating Geometry and the Unidirectional Ring Oscillator

OLIVER SANDFUCHS [†,*], **JÖRG LEONARDY** [†,1], **FRIEDEMANN KAISER** [†] **and MILIVOJ R. BELIĆ** [‡]

[†] Institute of Applied Physics—Nonlinear Dynamics, Darmstadt University of Technology, Hochschulstr. 4a, 64289 Darmstadt, Germany
[‡] Institute of Physics, P.O. Box 57, 11001 Belgrade, Yugoslavia

Abstract—We investigate spatio-temporal dynamics of two-wave mixing processes in a photorefractive medium, considering two different configurations. In the counterpropagating geometry, above a primary instability threshold we observe the onset of spontaneous spatial modulation of the Gaussian beam profile due to a static external electric field in the case of a self-focusing non-linearity. Running transverse waves in the optical near field and wandering spots in the far field occur when one transverse dimension is taken into account. Modulational inhomogeneities in the refractive index grating along the transverse direction result in beam focusing effects. In the copropagating wave mixing geometry within a unidirectional ring resonator we find four different mode-like structures with either symmetric or antisymmetric field distributions. Regular and irregular spatio-temporal oscillations arise for certain values of the resonator detuning. The temporal evolution of the chaotic mode oscillation is represented by a heteroclinic tangency and the spatio-temporal oscillation is characterized by crisis-induced intermittency.

1. INTRODUCTION

Structure formation in two- and four-wave mixing in photorefractive (PR) crystals has attracted considerable attention in recent years. Due to the non-linear interaction of light with PR media, a number of instabilities occurs leading to spatio-temporal dynamics in the transverse profile of the light beams and the formation of regular and irregular patterns. Since non-linear effects in PR crystals are significant even for very low laser intensities (of the order of mW/cm^2), it is easy to observe spatio-temporal patterns in this particular optical system. In addition, observation and detection of these patterns is simplified due to the fact that most commonly used PR media respond on a very slow time scale and thus structures evolve on the order of seconds or even minutes.

Two-wave mixing (2WM) can be considered as the elementary wave mixing process with respect to any other (higher order) wave mixing process. In this sense 2WM allows for two distinct interaction configurations: the counterpropagating geometry (Fig. 1a), where the interaction is dominated by reflection gratings, and the copropagating geometry, where the interaction is dominated by transmission gratings. In the latter geometry we supply the second beam through a feedback mechanism within a unidirectional ring resonator (Fig. 1b).

There have been two pioneering experiments on spatio-temporal structure formation in these 2WM geometries. The first one was done by Arecchi et al. in a unidirectional ring oscillator

*Corresponding author. E-mail: Oliver.Sandfuchs@physik.th-darmstadt.de
[1]Present address: Hewlett Packard GmbH, Herrenberger Str. 130, 71034 Böblingen, Germany

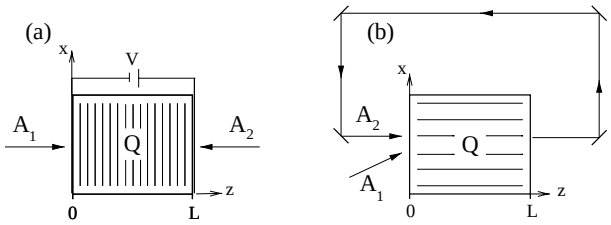

Fig. 1. Geometry of the two-wave mixing processes: (a) reflection geometry with an externally applied voltage V, (b) transmission geometry with a unidirectional ring cavity. z is the direction of propagation and x is the transverse dimension.

arrangement with a BSO-crystal and confocal mirrors [1]. They observed periodic alteration and chaotic itinerancy of transverse modes, depending on the value of the Fresnel number. In the following years a number of investigations of the unidirectional ring oscillator have been performed [2–4]. Theoretical explanations succeeded as far as the regular mode oscillation and the formation of phase singularities are concerned, but failed in explaining the transition to more complex spatio-temporal dynamics, owing to the lack of numerical methods for solving the coupled partial differential equations of the two- and four-wave mixing processes.

The other pioneering experiment was done by Honda [5], who reported on the spontaneous formation of hexagons in a $KNbO_3$-crystal in the reflection geometry. Theoretical investigations here were impeded by the fact that these structures occurred through reflection gratings, which are known to cause great difficulties for both analytical and numerical treatment. Theoretical predictions by means of linear stability analyses [6,7] offered improved understanding of the origin of structures, but could not reveal the spatio-temporal dynamics that occur above the primary instability threshold.

In this paper we present theoretical and numerical investigations of spatio-temporal structures that occur in these two distinct 2WM configurations. The goal is to identify similarities and differences in the spatio-temporal behaviour of these two systems, and to try to understand them in terms of simple concepts of non-linear dynamics.

2. MODEL EQUATIONS

The 2WM process is described by the propagation of two beams through a non-linear PR medium and their interaction with the medium. In the following we consider the standard photorefractive 2WM equations in paraxial approximation, of the form [8,9]

$$\partial_z A_1 + i f \partial_x^2 A_1 + \alpha A_1 = -Q A_2 \,, \tag{1a}$$

$$\pm\, \partial_z A_2 + i f \partial_x^2 A_2 + \alpha A_2 = Q^* A_1 \,. \tag{1b}$$

$A_{1,2}(x,z)$ are the slowly varying envelopes of the beams, f is a measure for the magnitude of diffraction, proportional to the inverse of the Fresnel number, and α is the absorption coefficient. The plus-minus sign in Eq. (1b) refers to the co- and contra-directional propagation of the second beam, respectively. The temporal evolution of the complex amplitude Q of the respective transmission or reflection grating in the crystal is approximated by a relaxation equation of the form [10]:

$$\tau \partial_t Q + \eta Q = \Gamma \quad \frac{A_1 A_2^*}{|\, A_1 \,|^2 + |\, A_2 \,|^2} \,. \tag{2}$$

τ is the relaxation time constant of the grating, η is a parameter dependent on internal electric fields of the crystal, and Γ is the PR coupling constant. This model includes the non-local and sluggish response of PR media, however all explicit spatial dependences in Q are neglected.

Equations (1) and (2) are solved numerically using our modified beam propagation method, described in [9]. The corresponding boundary conditions are chosen consistently with the common experimental conditions to be Gaussian beams in combination with "open" lateral sides (no reflecting or periodic boundaries). The longitudinal boundary conditions are specified in detail in Section 3 and 4.

3. THE REFLECTION GEOMETRY

In reflection geometry we are dealing with two-point boundary conditions at the opposite faces of the crystal. We choose Gaussian beam profiles in one transverse direction:

$$A_1(x, z = 0) = C_1 \exp(-x^2/w_0^2), \quad A_2(x, z = L) = C_2 \exp(-x^2/w_0^2)\,. \tag{3}$$

Here w_0 is the beam radius to which the transverse coordinate will be scaled. Since only the input intensity ratio $r_0 = I_1(0)/I_2(L)$ of the beams is a relevant parameter, we may put $C_1 = 1.0$ and $C_2 = r_0^{-1/2}$. In order to control the coupling strength of the crystal, we apply a static external electrical field $E_0 = V/L$ to the crystal in the direction of the grating wave vector. In this case we have, according to Kukhtarev et al. [10]:

$$\eta = \frac{E_d + E_q + iE_0}{E_M + E_d + iE_0}\,, \tag{4}$$

$$\Gamma = \Gamma_0 \left(1 + \frac{E_q}{E_d}\right) \frac{E_d + iE_0}{E_M + E_d + iE_0}\,, \tag{5}$$

with Γ_0 being the steady state coupling strength without external field. $E_d = 1$ kV/cm, $E_q = 5$ kV/cm and $E_M = 100$ kV/cm are the characteristic *internal* fields describing electronic processes in a $BaTiO_3$-crystal. E_0 will be scaled to E_d. Note that E_0 effectively renders both the coupling constant Γ and the relaxation time constant τ complex. Hence the external field E_0 exerts a profound influence on the process of wave mixing. By breaking the frequency degeneracy it allows for the build-up of running gratings and the appearance of running transverse waves. In this geometry the effect of absorption will be neglected.

3.1. *Linear stability of transverse modes*

The primary instability threshold for the onset of transverse patterns is determined by the linear instability of the steady-state plane-wave solutions. These steady-state plane-wave solutions ($f = 0$ and $\partial_t Q = 0$) were derived in Yeh [11] and, including absorption, in Belić [12]. They are the spatially homogeneous fixed-point solutions of the system. Their field amplitudes will be denoted by $A_1^0(z)$ and $A_2^0(z)$, and the corresponding amplitude of the refractive index grating by $Q^0(z)$. The stability analysis proceeds with a small perturbation of the wave and grating amplitudes:

$$A_1(z, x, t) = A_1^0(z)\,[1 + \epsilon a_1(z, x, t)]\,, \tag{6}$$

$$A_2(z, x, t) = A_2^0(z)\,[1 + \epsilon a_2(z, x, t)]\,, \tag{7}$$

$$Q(z, x, t) = Q^0(z)\,\big[1 + \epsilon q(z, x, t)\big]\,. \tag{8}$$

The perturbations a_1, a_2 and q will be expanded in the transverse Fourier ($x \to K$) and the temporal Laplace space ($t \to \lambda$). This yields an algebraic expression for q. After elimination of q, the linearized equations are cast in the common matrix form,

$$\partial_z \mathbf{a} = \mathcal{A}(z, K, \lambda)\, \mathbf{a}(z, K, \lambda)\,, \tag{9}$$

where $\mathbf{a} = (a_1, a_1^*, a_2, a_2^*)^T$. This non-autonomous equation cannot in general be solved analytically. The ratio of beams inside the crystal $r(z) = I_1^0(z)/I_2^0(z)$ is approximated by $r = 1$, which is quite good for strong couplings and a weak incident backward beam. With this constraint and a convenient choice of basis via a transformation $\mathcal{U}$, the perturbation matrix reads:

$$\mathcal{A} = \mathcal{U}^{-1} \begin{pmatrix} \gamma & -fK^2 & & \\ \beta + fK^2 & 0 & & \mathbf{0} \\ & & 0 & -h(\lambda) - fK^2 \\ & \mathbf{0} & fK^2 & g(\lambda) \end{pmatrix} \mathcal{U}\,. \tag{10}$$

The functions $g(\lambda) = \lambda[\Gamma_e\tau_e/(\lambda\tau_e + 1) + (\Gamma_e\tau_e)^*/(\lambda\tau_e^* + 1)]/2$ and $h(\lambda) = \lambda[\Gamma_e\tau_e/(\lambda\tau_e + 1) - (\Gamma_e\tau_e)^*/(\lambda\tau_e^* + 1)]/2\mathrm{i}$ appear because of the temporal variations in Q. γ and β are the real and imaginary parts of the effective complex coupling constant $\Gamma_e = \Gamma/\eta$, and $\tau_e = \tau/\eta$ is the effective complex PR time constant.

The formal solution of Eq. (9) is given by $\mathbf{a}(L) = \mathcal{F}(L)\mathbf{a}(0)$, where $\mathcal{F}(z) = \exp(\mathcal{A}z)$ is the linear flow matrix. The instability is determined by both the eigenvalues of $\mathcal{A}$ and the boundary conditions. Taking into account two-point boundary conditions, $\mathcal{F}$ is converted to a scattering matrix S, and we obtain the final form of the solution:

$$\mathbf{a}(z_{\mathrm{out}}) = S(K, \lambda)\, \mathbf{a}(z_{\mathrm{in}})\,, \tag{11}$$

where z_{out} and z_{in} are the output and the input faces of the crystal for the respective beams. The poles of the scattering matrix determine the nature and dynamics of an instability. In our case, the poles of S are found from the vanishing determinant of a 2×2 submatrix of $\mathcal{F}$, i.e. $\det(\mathcal{F}_{22}) = 0$. This condition gives the dispersion relation for a system of two counterpropagating light beams in a sluggish and non-local PR medium [13]:

$$\cosh\left(\frac{\gamma - g}{2}\right) + \cos(\chi_1)\cos(\chi_2) + p\ \mathrm{sinc}(\chi_1)\,\mathrm{sinc}(\chi_2) = 0\,, \tag{12}$$

where $\chi_1^2 = fK^2(fK^2 + \beta) - \gamma^2/4$, $\chi_2^2(\lambda) = fK^2(fK^2 + h) - g^2/4$, and $p(\lambda) = fK^2[fK^2 + (\beta + h)/2] + \beta h/2 + \gamma g/4$. Thus the stability analysis of a spatially extended system results in growth rates $\sigma = \Re(\lambda)$ for the transverse modes K, together with their oscillation frequencies $\Omega = \Im(\lambda)$. The instability threshold is inferred from the lowest lying branches of the marginal stability condition of the most unstable mode: $\sigma_{\max}(K; \Gamma_0, E_0) = 0$ (Fig. 2). As long as $|E_0|$ is small there is a region of stability for any transverse mode. The polarity of the external field determines the self-focusing properties of the medium. In the case of self-*de*focusing non-linearity ($E_0 > 0$), we encounter so-called *high-K-instability* that can either be due to the effects of linearizing the model equations or due to the model itself, and needs further investigation. In the case of self-focusing non-linearity ($E_0 < 0$), a finite band of transverse modes around the critical mode $fK_c^2 \approx 3.6$ is predicted to become unstable through a Hopf bifurcation at the critical value $E_0^c \approx -1.7$, with a characteristic oscillation frequency $\Omega_c\tau \approx 0.031$. The region where the instability balloon is displayed in Fig. 2 corresponds to a static instability. Its threshold, though, is always higher than that of the dynamic instability, and therefore is not observable. In addition, the slow medium response leads to plane-wave instabilities ($fK^2 = 0$) whose threshold is much higher than that for modal instabilities.

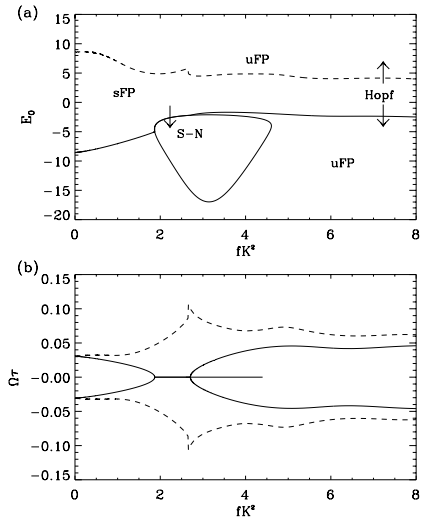

Fig. 2. (a) Threshold curves and (b) threshold frequency as functions of the transverse wave vector K. The solid curves are for $E_0 < 0$; dashed curves for $E_0 > 0$. "sFP" and "uFP" denote the regions of stable and unstable fixed points, respectively. "Hopf" and "S-N" (saddle node) indicate the nature of the bifurcation as the threshold curve is crossed in the direction of arrows.

3.2. *Spontaneous transverse intensity modulation*

For a self-focusing non-linearity linear stability analysis predicts the occurrence of transverse patterns above a primary threshold. In order to see what structures arise, we investigate the counterpropagating 2WM process by numerical simulation. In this and the subsequent sections we keep the following parameters constant

$$\Gamma_0 = 2.0\,, \quad r_0 = 20.09\,, \quad f = 2.5 \cdot 10^{-2}\,, \quad \alpha = 0\,.$$

The strength of the external field E_0 is our bifurcation parameter.

In our numerical simulations we find the threshold field strength to be somewhat higher ($E_0^c \approx -1.9$) than predicted, because the transverse modes were considered infinitely extended while performing stability analysis, whereas we deal with finite Gaussian beam profiles in our simulations. This may lead to discrepancies, but the approximation is good as long as the wavelength of modulation remains small enough compared to the beam waist. In Fig. 3 the transverse intensity profiles at the output faces of the crystal are shown at two subsequent times that are half an oscillation cycle apart, when the beam center either goes through its maximal or its minimal intensity.

Below threshold (Fig. 3a) we find the fixed point to be an attractor with a smooth Gaussian beam profile. Slightly above threshold (Fig. 3b) a spontaneous modulation of the beam profile appears. This modulation oscillates in time, and we find a limit cycle as an attractor. Its frequency, as well as the spatial frequency of the transverse modulation agree well with the values predicted by stability analysis.

With increasing field strength the amplitude of modulation increases until the beam center of I_1 drops and two regions of high intensity appear at the edges of the beam profile, whereas the center of beam I_2 steepens noticeably. These effects are due to beam focusing biased by the modulational instability in this 2WM geometry. Above threshold, along with the modulation of beam profiles an inhomogeneity in the refractive index emerges in the transverse dimension. The beams become focussed into the regions of high refractive index. This focusing is a dynamic

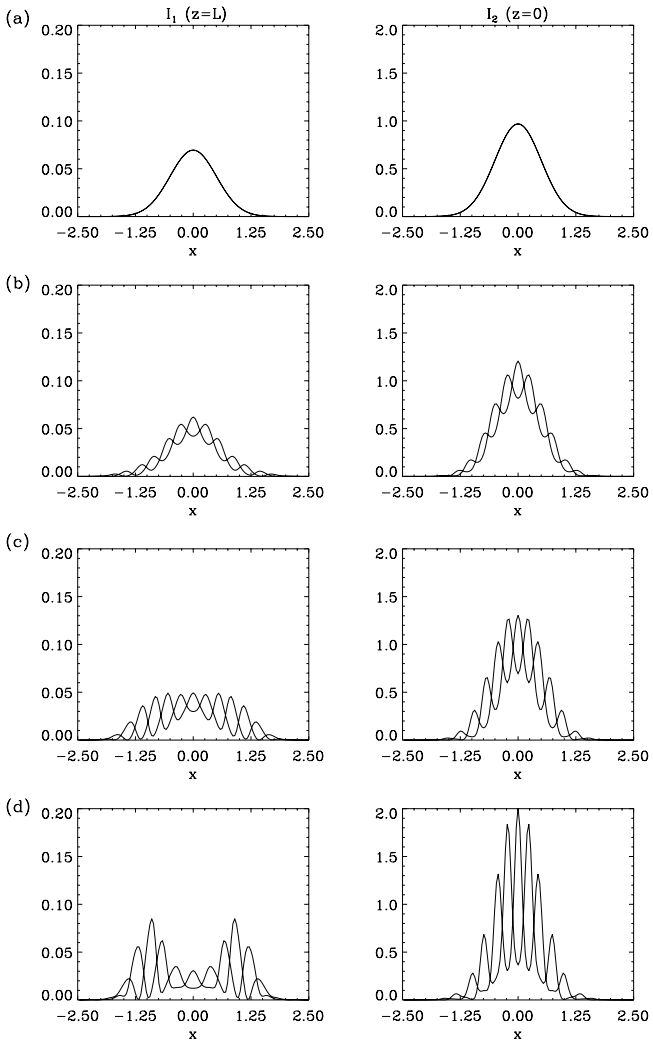

Fig. 3. Transverse intensity profiles for different E_0 in the self-focusing case: (a) -1.8, (b) -2.0, (c) -2.2, (d) -2.6.

process, because the index grating is a running grating.

If the transverse modulation in the beam intensity is plotted in time, as it is done for $I_1(z = L)$ in Fig. 4a, we recognize that it is not a standing, but a moving pattern. The transverse modulations seem to originate in the beam center, and a left-going and a right-going modulation runs across the beam profile, till either one disappears at the edges. Such spatio-temporal patterns are known as the *running transverse waves* [14]. This pattern occurs in the optical near field. Here it posesses a characteristic spatial length scale given by the critical wavelength $\Lambda_c = 2\pi/K_c$, which is in analogy to the well known roll pattern in one transverse dimension. In the far field these transverse patterns appear as two *wandering spots* (Fig. 4b) under a characteristic angle $\theta_c \approx K_c/k_z$ with respect to the direction of propagation z. They emerge as a pair of faint spots, become brighter while they move inward, and finally they fade away, and another pair begins to emerge.

In two transverse dimensions it is expected that the spots form patterns which appear as hexagonal or square lattices, depending on pattern selection criteria such as symmetries and

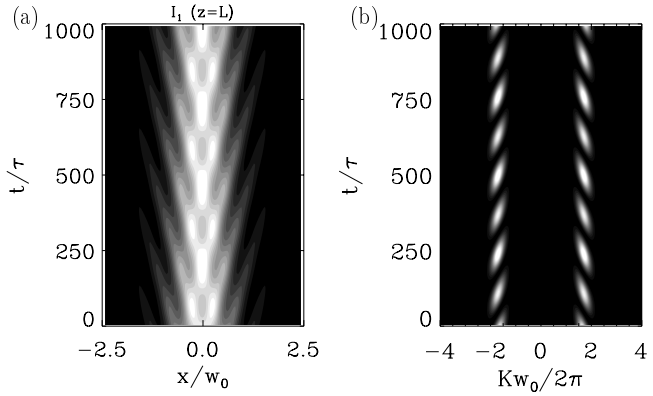

Fig. 4. Spatio-temporal dynamics of the intensity of the pump beam I_1 in one transverse dimension x slightly above the threshold at $E_0 = -2.0$: (a) Running transverse waves in the near field, corresponding to Fig. 3b, and (b) the corresponding wandering spots in the far field (here the pump beam is subtracted).

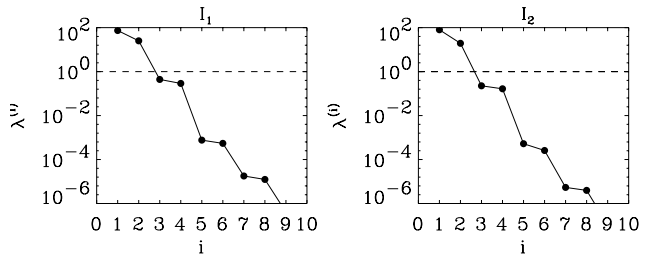

Fig. 5. Spectra of normalized eigenvalues $\lambda^{(i)}$ (in percent) for the intensity patterns of I_1 and I_2 with $E_0 = -2.0$.

boundary conditions. This has recently been seen in many experimental arrangements [5,15,16], where two counterpropagating optical beams have led to the spontaneous destabilization of the pump beams and thus to the spontaneous formation of transverse spatial patterns.

3.3. *Eigenmode analysis of running transverse waves*

In order to quantitatively characterize the spatial structures and their dynamics, we apply the singular value decomposition (SVD), also known as the Karhunen–Loève decomposition [14]. SVD was originally developed for the task of pattern recognition, but has generally proven powerful tool in determining and distinguishing different spatio-temporal degrees of freedom, which are most often hard to detect by visual inspection. By computing and analyzing the basic eigenmodes, we obtain a better insight into the mechanisms leading to complex spatio-temporal dynamics.

The procedure for SVD in principle performs a reduction of an intensity pattern $I(x,t)$ to its time averaged and its modulated parts. The intensity modulated part $\delta I(x,t) = I(x,t) - \langle I(x,t)\rangle_T$ is decomposed according to Karhunen and Loève into an orthogonal set of eigenmodes $\mathbf{p}^{(i)}(x)$ and their time dependent expansion coefficients $a^{(i)}(t)$ [14]:

$$I(x,t) = \langle I(x,t)\rangle_T + \sum_i a^{(i)}(t)\mathbf{p}^{(i)}(x)\,. \tag{13}$$

The eigenvalues $\lambda^{(i)}$ determine the probability of occurrence of the corresponding eigenvectors $\mathbf{p}^{(i)}$ in the intensity pattern $I(x,t)$. Figure 5 exhibits the spectra of the normalized eigenvalues

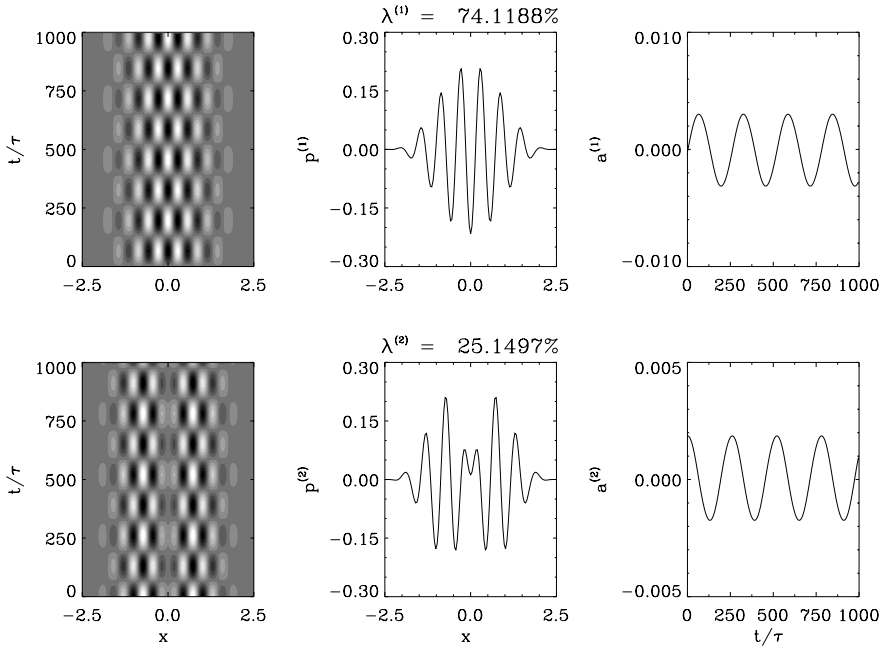

Fig. 6. Two dominating eigenmodes (middle column), their time dependent expansion coefficients (right column) and the corresponding substructures (left column) of the running transverse waves of Fig. 4a.

$\lambda^{(i)}$ for the intensity pattern of the running transverse waves in Fig. 4a. The eigenvalues decrease rapidly with increasing i. The two largest eigenmodes contain more than 99% of the original spatio-temporal information. Note that, as far as the order of magnitude is concerned, the eigenvalues are arranged in pairs.

In Fig. 6 the transverse dependence of two dominating eigenmodes, the time-series of expansion coefficients and the resulting spatio-temporal substructures $\delta I^{(i)}(x,t)$ are shown. Such a substructure by itself represents a *standing* transverse wave. The first eigenmode $p^{(1)}$ consists of a finite wavepacket with a basic spatial frequency K_0 and a temporal frequency Ω_0. The Fourier spectrum of the second eigenmode $p^{(2)}$ reveals that it contains the same temporal frequency Ω_0 and two basic spatial frequencies $K_1 = K_0 - \Delta K$ and $K_2 = K_0 + \Delta K$ that are separated by a frequency gap of $2\Delta K$. Both the transverse spatial structure as well as the temporal evolution of these two eigenmodes are shifted by $\pi/2$ relative to each other. This phase-shift allows the two standing wave patterns to combine to a running transverse wave. K_0 agrees well with the characteristic frequency K_c predicted by linear stability analysis and thus represents the transverse modulation due to the spontaneous destabilization of the homogeneous fixed-point solution. The occurrence of another frequency ΔK indicates a secondary bifurcation, which happens immediately after the primary bifurcation, and which we presume originates from the finite transverse Gaussian beam profile. In particular, it is responsible for the coexistence of a right-going and a left-going transverse wave, and the conservation of transverse symmetry with respect to the beam center.

4. THE UNIDIRECTIONAL RING RESONATOR

In the case of the unidirectional ring resonator one beam is fed back into the crystal and the input beams are given by:

$$A_1(x, z=0) = C_1 \exp(-x^2/w_0^2)\,, \quad A_2(x, z=0) = R\, \exp(ik_0\mathcal{L})\, \mathrm{FSP}[A_2(x, z=L)]\,. \tag{14}$$

where C_1 is the amplitude of the Gaussian pump beam incident upon the crystal and R is the overall reflectivity of the mirrors comprising the resonator. The term $k_0\mathcal{L}$ is the total propagation phase in free space

$$k_0\mathcal{L} = 2M\pi + \Psi_{\mathrm{ext}}\,, \tag{15}$$

with $-\pi \le \Psi_{\mathrm{ext}} \le \pi$ being the detuning of the external resonator. M is an integer number enumerating longitudinal modes. We pick Ψ_{ext} as the bifurcation parameter.

The *free space propagator* FSP is defined through [17]:

$$\mathrm{FSP}[A_2] = \mathrm{FT}^{-1}(\mathrm{FT}(A_2) \cdot \exp(if K^2\mathcal{L}))\,, \tag{16}$$

where FT (FT^{-1}) denotes the Fourier (the inverse Fourier) transform. In addition to the detuning of the resonator, there exists a detuning of the frequencies of waves relative to each other, $\delta\nu = \nu_1 - \nu_2$. For small values of $\delta\nu \approx 1 - 10$ Hz we may assume that both waves are subject to the same coupling constant Γ_0, although it needs to be modified to account for the build-up of a running grating:

$$\Gamma = \frac{\Gamma_0}{1 + 2\pi i\, \delta\nu\, \tau}\,. \tag{17}$$

Here Γ_0 is the PR coupling strength of the frequency degenerate wave mixing as it was introduced in Section 3. No external field is applied to the crystal in this configuration.

4.1. *Transverse mode-like structures*

Under the influence of diffraction within the medium one expects that different patterns arise in the transverse plane of the signal beam. Within the ring resonator there are no diffraction limiting apertures, nor curved mirrors. In an empty resonator there exist an infinite number of transverse modes. Which of these structures spontaneously emerge, and what their temporal evolution looks like, will be investigated here.

Without frequency detuning ($\delta\nu = 0$) one exclusively finds stationary solutions of the intracavity intensity for any value of Γ_0 and Ψ_{ext}. The intensity of the signal beam $I_{20} = I_2(z=0)$ attains a constant value, while the phase oscillates with a frequency Ω. The beam profiles in the transverse dimension remain Gaussian. In the subsequent discussion we take the following parameters

$$\Gamma_0 = 2.0\,, \quad R = 0.9\,, \quad f = 3 \cdot 10^{-4}\,, \quad \alpha = 0.1\,.$$

When a frequency detuning $\delta\nu = -0.47$ (in units of τ^{-1}) is present and the cavity detuning is in the range of $-0.05\pi \le \Psi_{\mathrm{ext}} \le 0.092\pi$, the situation is similar to the case $\delta\nu = 0$ and we observe a stationary Gaussian intensity profile. This structure is labelled "state 1" in Fig. 7a. It becomes different if we further increase Ψ_{ext}. Three additional transverse structures are observed, which we label "states $\bar{2}$, 3 and $\bar{4}$" (Figs. 7b–d). Their intensities I_{20} are still stationary. For $\Psi_{\mathrm{ext}} = 0.094\pi$ one observes a transverse beam profile consisting of two symmetric spots resembling a Gauss–Hermite mode of the first order (Fig. 7b). For the states 3 and $\bar{4}$ a bump and a dip emerges in between the symmetric spots.

Although I_{20} is constant in time, the frequency detuning results in an oscillation of the phases, similar to the one observed in the plane-wave limit. Fig. 8 displays the spatio-temporal dynamics of the real part of A_{20} for all four states. The oscillation frequency Ω is different for each state, and increases with increasing Ψ_{ext}. In Figs. 8b,d the real parts of the fields reveal an asymmetry with respect to the beam center, and therefore are labelled as "states $\bar{2}$ and $\bar{4}$". Their imaginary parts, of course, show identical but 90 degrees phase shifted oscillations.

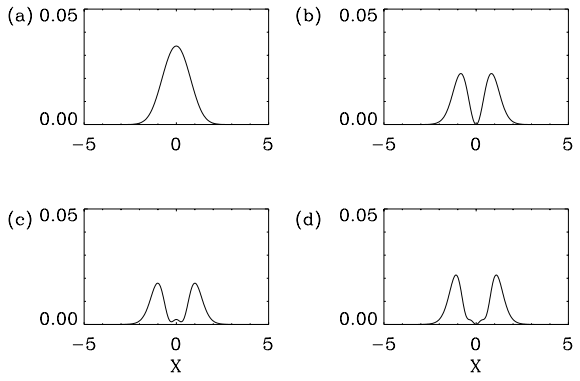

Fig. 7. Beam profiles of the signal beam $I_{20} = I_2\,(x, z = 0)$. (a) State 1 ($\Psi_{\text{ext}} = 0.091\pi$), (b) state $\bar{2}$ ($\Psi_{\text{ext}} = 0.094\pi$), (c) state 3 ($\Psi_{\text{ext}} = 0.097\pi$), and (d) state $\bar{4}$ ($\Psi_{\text{ext}} = 0.1\pi$).

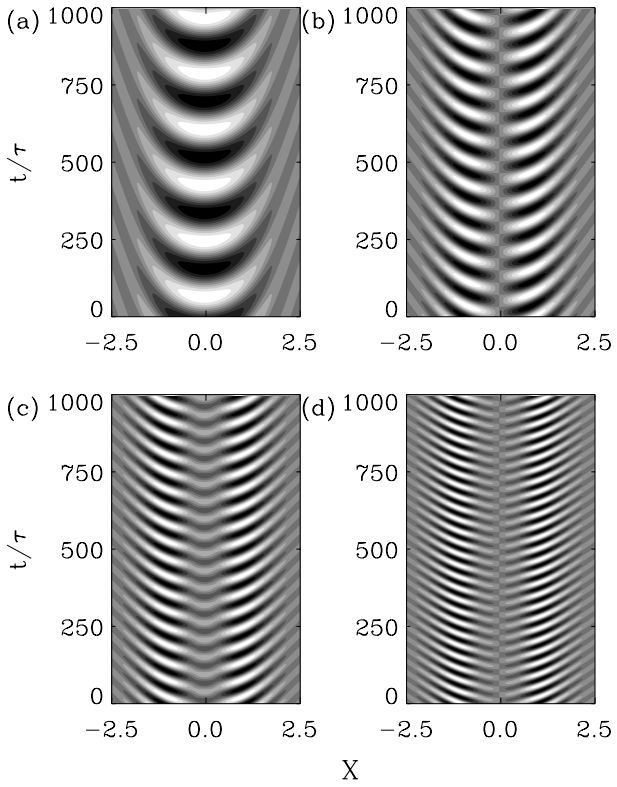

Fig. 8. Spatio-temporal dynamics of $\Re(A_{20})$. The simulations correspond to the stationary states shown in Fig. 7.

Despite the fact that there are no specific criteria prescribed for the selection of transverse modes in this resonator geometry, we observe low order Gauss-Hermite mode structures known from resonators with curved mirrors, as well as an alternating occurrence of symmetric and antisymmetric real and imaginary parts of the field I_{20} with higher mode index. They all arise spontaneously.

In a laser with curved mirrors the Gauss–Hermite modes become resonant when the atomic transition frequency and/or the resonator detuning is varied [18]. In analogy, one might have

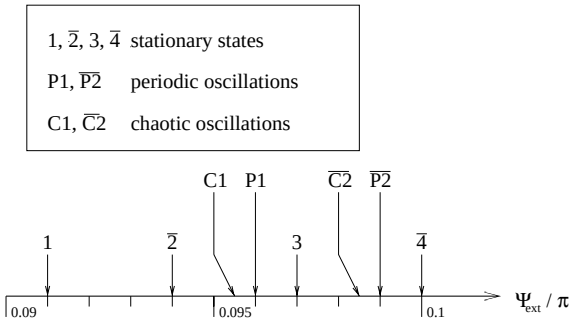

Fig. 9. Schematic representation of different spatio–temporal states by variation of the cavity detuning Ψ_{ext}. The bar denotes spatially antisymmetric states.

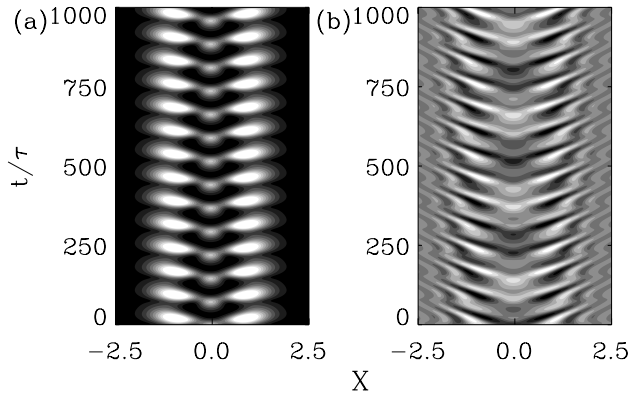

Fig. 10. Spatio-temporal dynamics of the periodic oscillation $P1$. (a) I_{20} and (b) $\Re(A_{20})$.

a similar understanding of the occurrence of stationary structures observed in this system. Variation of Ψ_{ext} changes the oscillation frequency Ω of the signal beam, hence a resonance appears with the oscillation frequencies of different transverse mode-like structures, i.e. the frequency Ω that is supported by the resonator lies within the gain line of one of the four stationary states. This state is favoured and the others are suppressed.

4.2. *Regular and irregular mode oscillations*

Besides the occurrence of stationary transverse mode-like structures, we observe regular and irregular spatio-temporal dynamics depending on the value of Ψ_{ext} in between the stationary states. A schematic overview of the bifurcation behaviour is shown in Fig. 9. Increasing Ψ_{ext} beyond the state $\bar{2}$, a chaotic oscillation (C1) followed by a periodic oscillation (P1) occurs. In between the symmetric state 3 and the antisymmetric state 4, a spatially antisymmetric and temporally chaotic state $\bar{C2}$, as well as a periodic state $\bar{P2}$ occur.

These periodic and chaotic states seem to be the superposition of two, not necessarily neighbouring, stationary states. In order to see this we have plotted the spatio-temporal dynamics of the periodic state P1 in Fig. 10. In the intensity I_{20} two latteral spots oscillate synchronously and alternatingly with a faint central spot. In the real part of A_{20} one sees two oscillating patterns: a pattern from the state 3, as in Fig. 8c, which is superimposed on the pattern from state 1, as in Fig. 8a. The power spectrum of state P1 (Fig. 11) reveals two dominant frequency lines, which approximately coincide with the frequencies Ω_1 and Ω_3 of the herein involved stationary state

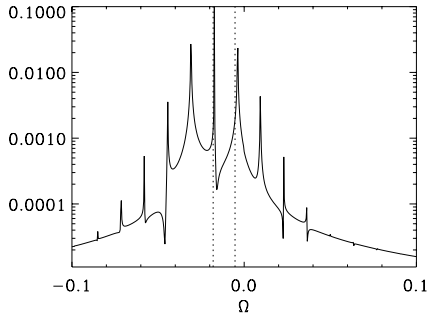

Fig. 11. Power spectrum (arbitrary units) of the periodic oscillation $P1$ of Fig. 10. The spectrum is calculated for the complex electric field $A_{20}(x = -0.74, t)$ and the frequency Ω is given in units of $1/\tau$. Dashed lines represent the frequencies of the stationary oscillation of the state 1 ($\Omega = -0.0053$) and of the state 3 ($\Omega = -0.018$), respectively.

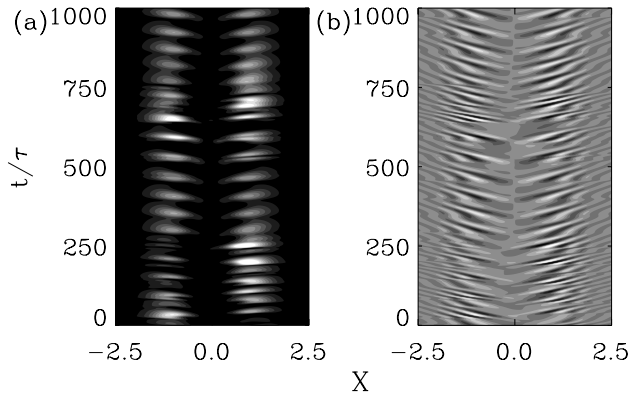

Fig. 12. Spatio-temporal dynamics of the chaotic oscillation $\bar{C}2$. (a) I_{20} and (b) $\Re(A_{20})$.

patterns 1 and 3. Other frequency lines in the spectrum are higher harmonics of the frequency difference $\Omega_1 - \Omega_3$. This regular mode oscillation can therefore be understood as a phenomenon called *mode-beat*.

Similar behaviour holds for the chaotic state $\bar{C}2$. It is an antisymmetric state, as antisymmetric beating dominates the pattern. The intensity pattern consists of two spots which alternatingly oscillate asynchronously and synchronously (Fig. 12). In the power spectrum (Fig. 13) broadband continuous spectrum dominates, with a few frequency lines visible, coinciding approximately with the frequencies Ω_2 and Ω_4, and some harmonics of the frequency difference.

4.3. *Complex eigenmode analysis of mode oscillations*

By means of the eigenmode analysis discussed in Section 3.3, one obtains information about the spatio-temporal behaviour of involved substructures. Moreover, an eigenmode analysis of the complex field amplitudes provides information on the symmetry of the substructural patterns [19], which in our case are the symmetric and antisymmetric mode-like structures.

In Fig. 14. 14 the real and imaginary part (left column) and the intensity (right column) of the four largest eigenmodes $\mathbf{p}^{(i)}(x)$ of the chaotic state $C2$ are displayed. The first and third eigenmodes correspond to an antisymmetric, and the second and forth eigenmode to a symmetric substructure. The intensities are represented again by two spots. The sum of the eigenvalues $\lambda^{(i)}$

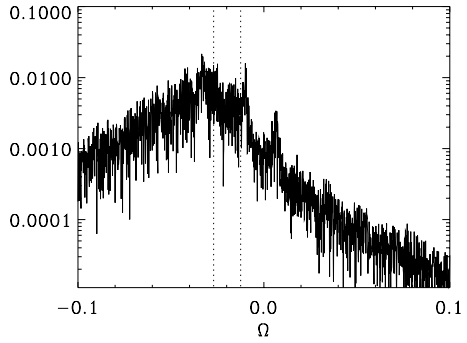

Fig. 13. Power spectrum (arbitrary units) of the chaotic oscillation $\bar{C}2$ of Fig. 12. The spectrum is calculated for the complex electric field $A_{20}(x = -0.74, t)$, and the frequency Ω is given in units of $1/\tau$.

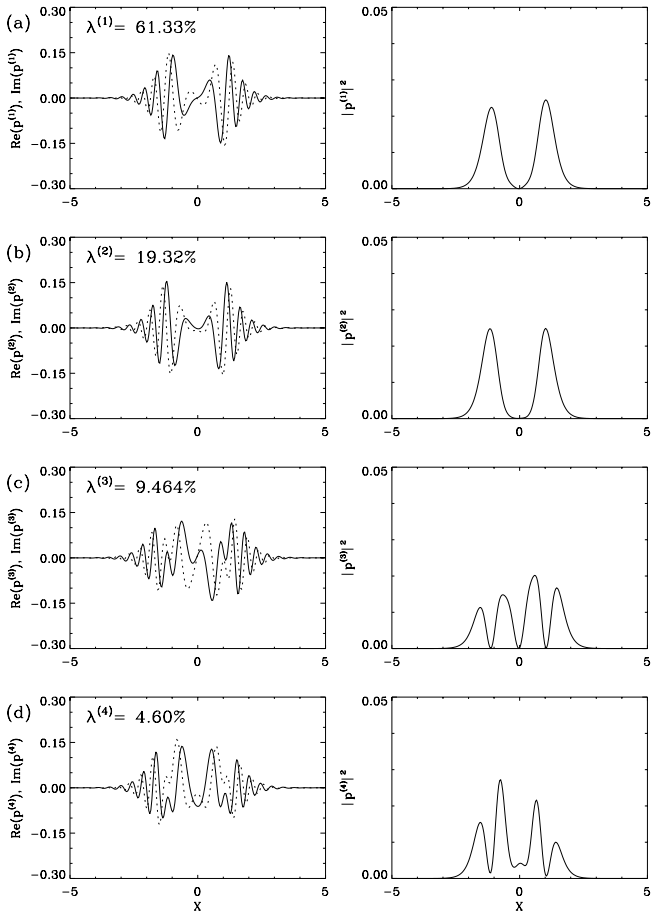

Fig. 14. Complex eigenmodes of the chaotic oscillation $\bar{C}2$ of Fig. 12. Left: real- and imaginary parts of the eigenmodes $\mathbf{p}^{(i)}(x)$. Right: the corresponding moduli $|\mathbf{p}^{(i)}|^2$.

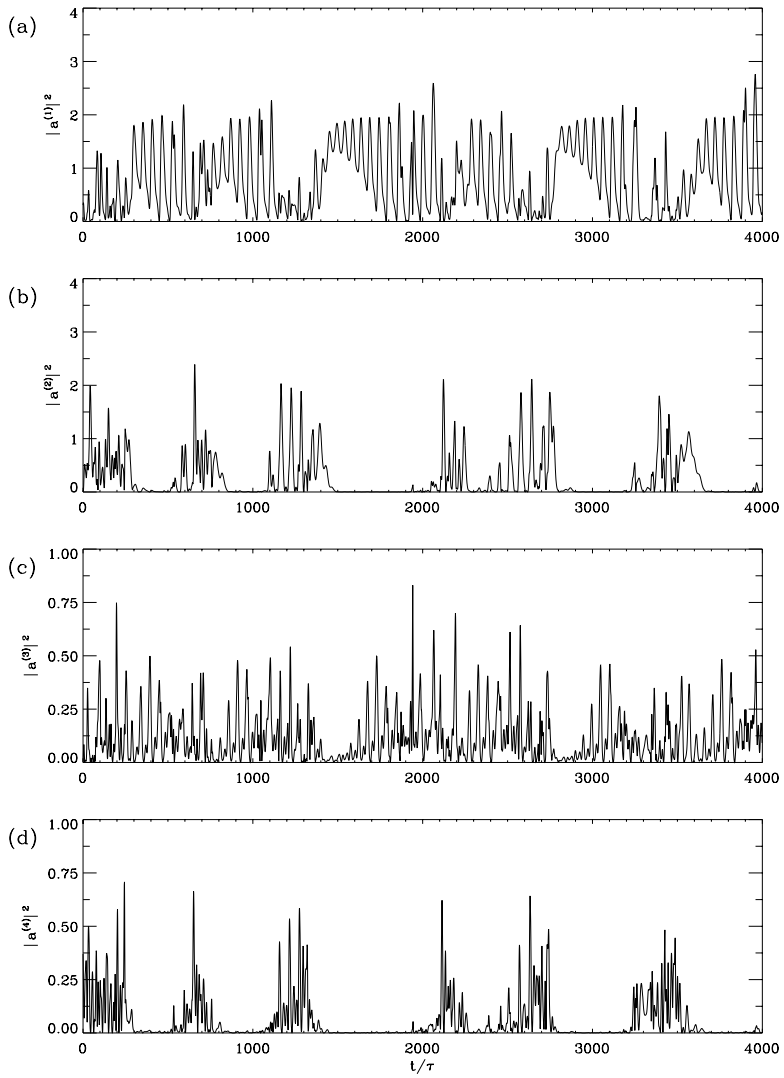

Fig. 15. Time expansion coefficients $|a^{(i)}|^2$ of the complex eigenmodes of Fig. 14.

of these four eigenmodes is larger than 95%, so they contain most of the essential information of the structure. The higher eigenmodes contribute small corrections.

The irregular temporal evolution of the eigenmodes ($|a^{(i)}(t)|^2$) explains the dynamics of $\bar{C}2$ (Fig. 15). The coefficient $|a^{(1)}(t)|^2$ represents a periodic (laminar) oscillation in different time intervals, displaying synchronous oscillation of the spots (see Fig. 12). Within such laminar intervals the amplitude of oscillation increases, becomes irregular and finally collapses. At that moment $|a^{(2)}(t)|^2$ emerges, and lasts until another laminar interval of $|a^{(1)}(t)|^2$ sets in. $|a^{(3)}(t)|^2$ shows an irregular temporal behaviour, however the signal $|a^{(4)}(t)|^2$ is nearly synchronized with the sequence of bursts of $|a^{(2)}(t)|^2$. Hence, this eigenmode analysis again justifies the notion of $\bar{C}2$ as being an antisymmetric state.

Such a dynamical behaviour points towards a process termed *crisis-induced intermittency* [20], which here is due to a boundary crisis. In the boundary crisis there exists a *heteroclinic tangency* between two unstable solutions. For different time intervals the system oscillates in the basin

of an unstable solution, represented in this case by $\mathbf{p}^{(1)}$. Following the heteroclinic tangential orbit, the system comes close to the basin of another unstable orbit (here $\mathbf{p}^{(2)}$) and stays there for some time, before reaching again the basin of attraction of the first orbit, and so on, with a temporally irregular repetition.

In order to identify this type of bifurcation as crisis-induced intermittency, it is necessary to investigate the dependence of the mean length $< l >$ of intervals with vanishing spatial symmetry breaking on the bifurcation parameter Ψ_{ext}. This, however, would require much longer time series than the ones shown here. Even in the present form numerical simulations require a massive computational support.

5. CONCLUSIONS

Two different two-wave mixing configurations have theoretically been investigated with respect to their spatio-temporal dynamics in one transverse dimension.

In the case of counterpropagating two-wave mixing, a linear stability analysis has been performed, predicting the onset of spontaneous destabilization of the homogeneous steady-state solution. We found that an externally applied electric field always results in dynamic instabilities via Hopf-bifurcation, due to the removal of frequency degeneracy in the two-wave mixing process. Above the primary instability threshold, in our numerical simulations we observed the occurrence of running transverse waves in the optical near field, and wandering spots in the far field. The temporal frequency of the limit cycle oscillation, as well as the spatial frequency of the transverse modulation agree well with the values predicted by stability analysis. Above the threshold, refractive index inhomogeneities cause transverse focusing effects. An eigenmode analysis revealed the running transverse waves as the secondary instabilities.

In the case of the unidirectional ring oscillator, the occurrence of four different transverse structures similar to Gauss-Hermite modes have been observed, depending on the resonator detuning. These structures either possess symmetric or antisymmetric field distributions. Regular and irregular mode oscillations are found, which are shown to be a dynamic superposition of two mode-like structures. Such superposition results in the appearance of two wandering spots in the intracavity field (with or without an accompanying central peak) which perform periodic and aperiodic motion. A complex eigenmode analysis allows us to determine the symmetry of the complex spatial field modes. As far as the spatio-temporal dynamics is concerned, appart from periodic mode beatings, a heteroclinic tangency between a symmetric and an antisymmetric mode oscillation is observed, leading to spatio-temporal chaos. The temporal evolution displays the characteristic behaviour of crisis-induced intermittency. Our numerical simulations are in general qualitative agreement with experimental results [3,4,21], where also superpositions of a few low order Gauss-Hermite or Gauss-Laguerre mode-like structures are found to dominate the spatio-temporal dynamics of the intracavity field.

We plan to extend the simulations to two transverse dimensions, which we have already done for four-wave mixing geometries in optical phase conjugation [14,22]. In Ref. [22] the spatio-temporal dynamics of a *bidirectional* ring oscillator, which is governed by a four-wave mixing process, has numerically been investigated.

Acknowledgement—Work at the Institute of Applied Physics (Darmstadt University of Technology) is financially supported within the Sonderforschungsbereich 185 "Nichtlineare Dynamik" of the *Deutsche Forschungsgemeinschaft*. Work at the Institute of Physics (Belgrade) is supported by the Project 01M07 of the Ministry of Science and Technology of the Republic of Serbia. We would like to thank Markus Münkel and Andreas Stepken for valuable and interesting discussions.

REFERENCES

1. Arecchi, F. T., Giacomelli, G., Ramazza, P. L. and Residori, S., *Experimental evidence of chaotic itinerancy and spatiotemporal chaos in optics*, Phys. Rev. Lett., 1990, **65**, 2531–2534.
2. D'Alessandro, G., *Spatiotemporal dynamics of a unidirectional ring oscillator with photorefractive gain*, Phys. Rev. A, 1992, **46**, 2791–2802.
3. Hennequin, D., Dambly, L., Dangoisse, D. and Glorieux, P., *Basic transverse dynamics of a photorefractive oscillator*, J. Opt. Soc. Am. B, 1994, **11**, 676–683.
4. Jost, B. M. and Saleh, B. E. A., *Complex Ginzburg–Landau and extended Kuramoto–Sivashinsky equations for unidirectional photorefractive ring resonators*, Phys. Lett. A, 1995, **205**, 44–50.
5. Honda, T., *Hexagonal pattern formation due to counterpropagation in $KNbO_3$*, Opt. Lett., 1993, **18**, 598–600.
6. Saffman, M., Zozulya, A. A. and Anderson, D. Z., *Transverse instability of energy exchanging counterpropagating two-wave mixing*, J. Opt. Soc. Am. B, 1994, **11**, 1409–1417.
7. Honda, T. and Banerjee, P. P., *Threshold for spontaneous pattern formation in reflection-grating-dominated photorefractive media with mirror feedback*, Opt. Lett., 1996, **21**, 779–781.
8. Belić, M. R., Leonardy, J., Timotijević, D. and Kaiser, F., *Transverse Effects in Double Phase Conjugation*, Opt. Commun., 1994, **111**, 99–104.
9. Belić, M. R., Leonardy, J., Timotijević, D. and Kaiser, F., *Spatiotemporal Effects in Double Phase Conjugation*, J. Opt. Soc. Am. B, 1995, **12**, 1602–1616.
10. Kukhtarev, N. V., Markov, V. B., Odulov, S. G., Soskin, M. S. and Vinetskii, V. L., *Holographic storage in electrooptic crystals. I. Steady state*, Ferroelectrics, 1979, **22**, 949–960.
11. Yeh, P., *Contra-Directional Two-Wave Mixing in Photorefractive Media*, Opt. Commun., 1983, **45**, 323–326.
12. Belić, M. R., *Comment on using the shooting method to solve boundary-value problems involving coupled-wave equations*, Opt. Quantum Electron., 1984, **16**, 551–557.
13. Sandfuchs, O., Leonardy, J., Kaiser, F. and Belić, M. R., *Transverse instabilities in photorefractive counterpropagating two-wave mixing*, Opt. Lett., 1997, **22**, 498–500.
14. Leonardy, J., Kaiser, F.. Belić, M. R. and Hess, O., *Running Transverse Waves in Optical Phase Conjugation*, Phys. Rev. A, 1996, **53**, 4519–4527.
15. Banerjee, P. P., Yu, H.-L., Gregory, D. A., Kukhtarev, N. and Caulfield, H. J., *Self-organization of scattering in photorefractive $KNbO_3$ into a reconfigurable hexagonal spot array*, Opt. Lett., 1995, **20**, 10–12.
16. Mamaev, A. V. and Saffman, M., *Hexagonal optical patterns in anisotropic non-linear media*, Europhys. Lett., 1996, **34**, 669–674.
17. Moloney, J. V., Belić, M. R. and Gibbs, H. M., *Calculation of transverse effects in optical bistability using fast fourier transform techniques*, Opt. Commun., 1992, **41**, 379–382.
18. Brambilla, M., Battipede, F., Lugiato, L. A., Penna, V., Prati, F., Tramm, C. and Weiss, C. O., *Transverse Laser Patterns, I. Phase singularity crystals*, Phys. Rev. A, 1991, **43**, 5090–5113.
19. Münkel, M., Hess, O. and Kaiser, F., *Stabilization of spatio-temporally chaotic semiconductor laser arrays by means of delayed optical feedback*, Phys. Rev. E, 1997, **56**, 3868–3875.
20. Grebogi, C., Ott, E., Romeiras, F. and Yorke, J. A., *Critical exponents for crisis-induced intermittency*, Phys. Rev. A, 1987, **36**, 5365–5380.
21. Korwan, D. R. and Indebetouw, G., *Experimental modal analysis of the spatiotemporal dynamics of a linear photorefractive phase-conjugate resonator*, J. Opt. Soc. Am. B, 1996, **13**, 1473–1481.
22. Leonardy, J., *Raum-zeitliche Dynamik photorefraktiver Oszillatoren*, Doctoral Thesis at the Institute of Applied Physics, Darmstadt University of Technology, 1997.